Original Article

# Assessment of intratumor heterogeneity for preoperatively predicting the invasiveness of pulmonary adenocarcinomas manifesting as pure ground-glass nodules

**Hongliang Qi[1#], Zhichao Zuo[2#], Shanyue Lin[3#], Ye Chen[1], Hanwei Li[1], Debin Hu[1], Yingjun Zhou[4], Wanyin Qi[5], Hongwen Chen[1]**

[1]Department of Clinical Engineering, Nanfang Hospital, Southern Medical University, Guangzhou, China; [2]School of Mathematics and Computational Science, Xiangtan University, Xiangtan, China; [3]Department of Radiology, Affiliated Hospital of Guilin Medical University, Guilin, China; [4]Department of Radiology, Xiangtan Central Hospital, Xiangtan, China; [5]Department of Radiology, The Affiliated Hospital, Southwest Medical University, Luzhou, China

*Contributions:* (I) Conception and design: H Qi, Z Zuo; (II) Administrative support: Y Chen, H Chen, H Li; (III) Provision of study materials or patients: Z Zuo, S Lin; (IV) Collection and assembly of data: W Qi, Z Zuo, D Hu, Y Zhou; (V) Data analysis and interpretation: Z Zuo; (VI) Manuscript writing: All authors; (VII) Final approval of manuscript: All authors.

[#]These authors contributed equally to this work.

*Correspondence to:* Wanyin Qi, MB. Department of Radiology, The Affiliated Hospital, Southwest Medical University, No. 25 Taiping Street, Jiangyang District, Luzhou 646000, China. Email: qiwanyin0508@163.com; Hongwen Chen, MM. Department of Clinical Engineering, Nanfang Hospital, Southern Medical University, 1023 Shatai Road, Baiyun District, Guangzhou 510515, China. Email: chw47922@126.com.

**Background:** The increased use of low-dose computed tomography (CT) for lung cancer screening has improved the detection of ground-glass nodules. However, as the clinical utility of CT findings to predict the invasiveness of pure ground-glass nodules (pGGNs) is currently limited, differentiating pGGNs that indicate invasive adenocarcinoma (IAC) from those that represent other histological entities is challenging. We aimed to quantify intratumor heterogeneity of lung adenocarcinomas characterized by pGGNs on CT to assess its efficacy in predicting IACs before surgery.

**Methods:** Overall, 575 patients with persistent pGGNs and a postoperative pathological diagnosis of lung adenocarcinoma were included. To quantitatively measure intratumor heterogeneity, an intratumor heterogeneity score that incorporated local radiomics features and global pixel distribution patterns was developed. Accuracy of the preoperative prediction of pathological invasiveness was evaluated using the area under the receiver operating characteristic (ROC) curve. The performance of the intratumor heterogeneity score was compared with that of radiomics features and conventional imaging findings.

**Results:** Conventional imaging findings yielded area under the curve values of 0.832 and 0.842 for the training and validation cohorts, respectively. The performance of imaging findings was inferior to that of radiomics, which yielded area under the curve values of 0.868 and 0.879 for the training (P=0.008) and validation (P=0.007) cohorts, respectively. Similarly, the performance of imaging findings was inferior to that of the intratumor heterogeneity score, with area under the curve values of 0.860 and 0.867 for the training (P=0.019) and validation (P=0.045) cohorts, respectively. The diagnostic performance of the intratumor heterogeneity score was comparable to that of radiomics features, with no significant difference between their ROC curves (training: P=0.635; validation: P=0.686).

**Conclusions:** The performance of the intratumor heterogeneity score was comparable to that of radiomics features and superior to that of conventional imaging findings for the preoperative prediction of the IACs that present as pGGNs.

**Keywords:** Intratumor heterogeneity score (ITH score); invasiveness; pulmonary adenocarcinomas; pure ground-glass nodule (pGGN); prediction

Submitted Apr 10, 2024. Accepted for publication Nov 06, 2024. Published online Dec 24, 2024.
doi: 10.21037/qims-24-734
**View this article at:** https://dx.doi.org/10.21037/qims-24-734

## Introduction

The increased use of low-dose computed tomography (CT) for lung cancer screening has improved the detection of ground-glass nodules (GGNs), which can be classified into mixed GGNs (mGGNs) and pure GGNs (pGGNs) (1,2). Unlike solid nodules, GGNs are commonly associated with lung adenocarcinoma (3). Specifically, pGGNs are characterized by a more indolent nature, slower growth, and a lower likelihood of progression to lung adenocarcinomas (4,5). Even when pGGNs are malignant, the postoperative pathology is more likely to indicate atypical adenomatous hyperplasia (AAH), adenocarcinoma in situ (AIS), or minimally invasive adenocarcinoma (MIA) and less likely to indicate invasive adenocarcinoma (IAC) (6-9). Although many pGGNs have an indolent course, most are diagnosed pathologically as IAC, with incidence rates ranging from 35.4% to 44.2% (10-12). The 10-year disease-free survival rate after complete resection for patients with AIS and MIA is 100% (13), whereas the 5-year survival rate after complete resection for patients with IAC is 89% (14). Treatment for IAC requires a more extensive approach than does that for AAH/AIS and MIA. Therefore, although segmentectomy or wedge resection is often considered sufficient for the surgical management of AAH/AIS and MIA (15), segmentectomy is typically the most appropriate treatment for IAC (16).

CT is a noninvasive imaging modality that can be used to predict tumor invasiveness preoperatively, with nodule size and attenuation being important characteristics of invasiveness (17-21). Other morphological features that have been explored include margins, air bronchograms, bubble appearance, spiculation, lobulation, and pleural indentation (22-24). However, studies have reported conflicting results and histological overlap, which is attributable to the subjectivity of interpretations and the influence of inexperience or infrequent observations. As the clinical utility of CT parameters to predict the invasiveness of pGGNs is currently limited, differentiating between pGGNs indicative of IAC from those representing other histological entities remains challenging.

CT-based radiomics approach, which involves a high-throughput quantitative analysis of medical imaging, can facilitate treatment decisions in lung cancer by generating a comprehensive array of quantitative imaging features that significantly surpass the interpretative capabilities of radiologists, thereby addressing the limitations of the clinical utility of CT parameters (25). Numerous CT-based radiomics prediction models have been developed to distinguish between IAC and AIS/MIA with pulmonary adenocarcinomas that present as pGGNs (26-29).

However, traditional radiomics primarily focus on the entire tumor region, thereby overlooking intratumoral heterogeneity (ITH) resulting from factors such as angiogenesis, metabolism, and proliferation. These factors are influenced by the diversity in the populations of tumor cells and stromal components, as well as their uneven distribution within intratumoral subregions (30). Furthermore, predefined radiomics features are typically centered on local pattern frequencies, such as co-occurring gray levels, with no evaluation of subregional variations, and thus subregional distributions are ignored (31-33). Consequently, to perform a comprehensive assessment of tumor heterogeneity, it is crucial to simultaneously consider pixel characteristics and their spatial distributions. Introducing the ITH score represents a significant step toward capturing multiscale ITH information through the concurrent integration of local and global radiomics data (31-33). For instance, Li *et al.* (32) established a correlation between the ITH score and the biological behaviors that influence the prognosis for patients with non-small cell lung cancer (e.g., lymphovascular and pleural invasion).

Therefore, in this study, we used the ITH score to evaluate pulmonary adenocarcinomas presenting as pGGNs to differentiate between IAC and AIS/MIA and thus better guide the clinical management of pGGNs and surgical planning. We present this article in accordance with the TRIPOD reporting checklist (available at https://qims.amegroups.com/article/view/10.21037/qims-24-734/rc).

## Methods

### *Ethical approval*

This study was conducted in compliance with the Helsinki Declaration (as revised in 2013). Ethical approval for this multicenter, cancer registry-based study was obtained from the institutional ethics committees of the Xiangtan Central Hospital (No. 2021-07-009), Affiliated Hospital of Guilin Medical University (No. 2023YJSLL-121), and the Affiliated Hospital of Southwest Medical University (No. KY2020147). Given the retrospective design of the study, the necessity for obtaining written informed consent from participants was waived.

### *Study population*

This study encompassed a cohort of 937 patients presenting with persistent pGGNs, all of whom underwent curative surgical resection followed by a postoperative pathological diagnosis of lung adenocarcinoma. The patient data, collected from January 2019 to January 2023, were sourced from the medical facilities of Xiangtan Central Hospital, the Affiliated Hospital of Guilin Medical University and the Affiliated Hospital of Southwest Medical University. Pathological diagnoses were classified in accordance with the adenocarcinoma guidelines established by the International Association for the Study of Lung Cancer, the American Thoracic Society, and the European Respiratory Society (15). A comprehensive review of patients' medical records, including clinical characteristics (age and sex), preoperative chest CT imaging findings, and pathological diagnoses, was conducted.

Solid pulmonary nodules were defined as completely solid soft-tissue density lesions on preoperative chest CT images. mGGNs included nodules with a pure ground-glass appearance and part-solid density, whereas pGGNs were defined as foci of decreased density attenuation in which the cross-section of the bronchus and vessels could be observed on thin-section CT images (1,2). In this study, pulmonary adenocarcinomas that manifested as pGGNs were further analyzed.

The inclusion criteria were as follows: identification of lesions as pGGNs via high-resolution preoperative CT; maximum nodule diameter ranging from 0.5 to 3 cm; and no history of biopsy, chemotherapy, or radiotherapy before the CT evaluation. The following exclusion criteria were applied: poor image quality attributable to artifacts, a time interval of more than 2 weeks between CT scan and surgery, and the presence of severe and concurrent chronic conditions such as malignancies. The procedural workflow is illustrated in *Figure 1*. Ultimately, 575 patients were enrolled in the study and subsequently randomized into training and validation cohorts in a 7:3 ratio. For patients exhibiting multiple pGGNs on CT images, only the nodule with a confirmed pathological diagnosis was included in the subsequent analysis.

### *CT examinations*

Chest CT examinations were conducted using nine computed tomography machines from four prominent manufacturers: GE Medical Systems (Waukesha, Wisconsin, USA), Siemens Healthineers (Erlangen, Germany), Philips (Amsterdam, Netherlands), and United Imaging Healthcare (Shanghai, China). The parameters for image acquisition during the CT scan were as follows: tube voltage, 120 kVp; tube current-time product, 170–200 mA; matrix, 512 × 512; and slice thickness, 1–5 mm. Additionally, beam pitches of 0.515 and 0.758 were used with standard resolution algorithms as integral components of the scanning process.

### *Conventional imaging findings*

Two skilled radiologists, blinded to the diagnosis, methodically assessed the semantic characteristics of all CT images obtained with a lung window [level −700 to −500 Hounsfield units (HU); width 1,500 to 2,000 HU]. The evaluation criteria included tumor location, margins, lobulation, spiculation, vacuole signs, vascular convergence signs, and pleural indentation. Additionally, we measured the CT value three times on the two-dimensional maximum axial slice and calculated the mean value from areas that covered most of the pGGNs while ensuring that these areas did not include vessels, bronchi, or air-filled cavities. Lesion size was determined by identifying the maximum diameter in the axial plane according to the guidelines outlined in the eight edition of the TNM staging protocols (15).

### *Image preprocessing*

To address the variability of CT scanner devices and parameters, including differences in slice thickness, we implemented a comprehensive image preprocessing pipeline. This pipeline included several key steps. First, image resampling was conducted using the "PyRadiomics" package in Python 3.11.0 (Python Software Foundation,

 

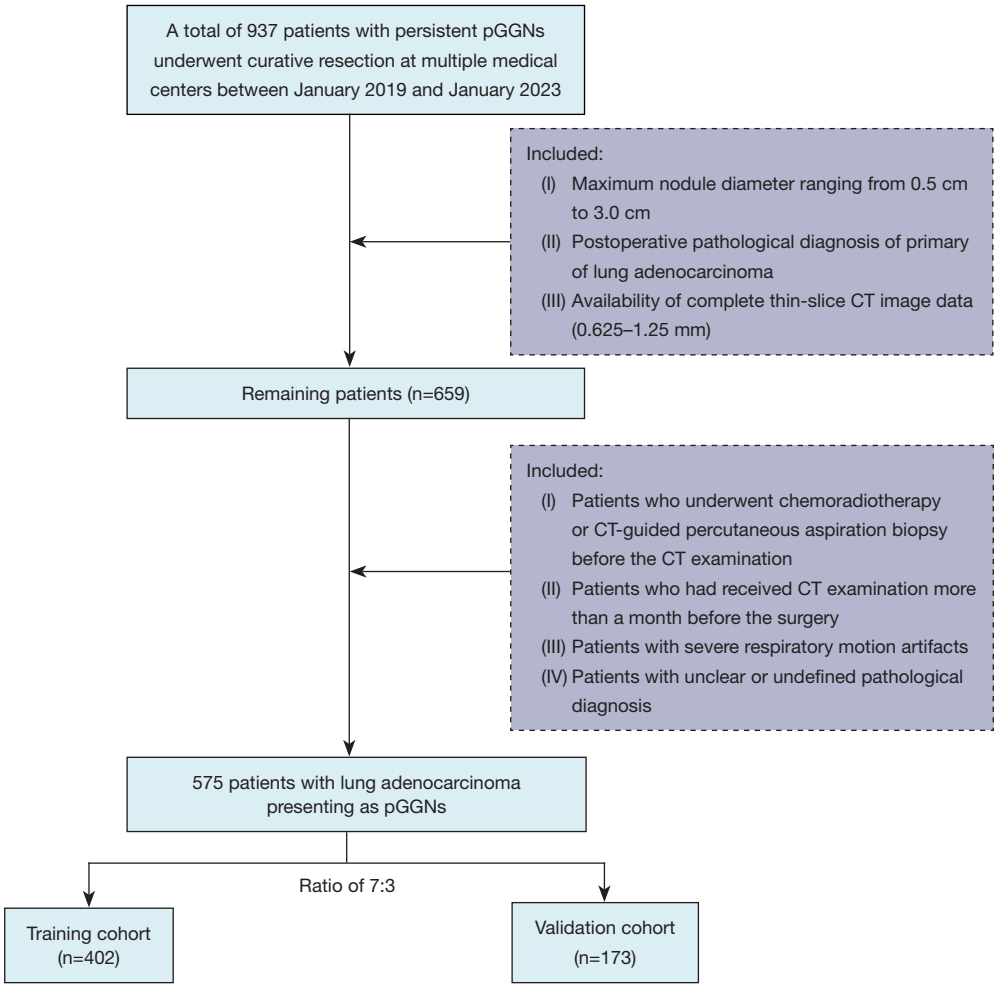


**Figure 1** Overview of the study's procedural flow. CT, computed tomography; pGGNs, pure ground-glass nodules.

Wilmington, DE, USA), standardizing the voxel dimensions to 1×1×1 $mm^3$ (X, Y, Z). The resampling algorithm employed a B-spline curve with a sitkBSpline interpolator with a parameter value of 3 to ensure smooth and accurate interpolation of the image data. Subsequently, we modified the bin width to partition the pixel intensity range of 0–255 into five discrete intervals. This binning approach effectively discretized the intensity values, reducing the dimensionality of the feature space and facilitating subsequent analysis.

### *Construction of the radiomics model*

The construction of the radiomics model involved the following essential steps: nodule segmentation, feature extraction, feature reduction, and radiomics score (Rad score) calculation. ITK-SNAP software version 4.0.2 was used to segment the nodules in all CT images. Initially, the lesion was manually delineated by a junior trainee radiologist with 5 years of experience in thoracic imaging. Subsequently, a senior radiologist with 15 years of expertise reviewed and adjusted the segmentations.

The "PyRadiomics" package in Python 3.11.0 was used to extract 1,239 radiomics features from the pGGN area, including first-order features; histogram features; and texture features, such as the gray-level run length matrix, gray-level co-occurrence matrix, and gray-level size zone matrix. During the feature reduction stage, the minimum redundancy-maximum relevance method was initially implemented to address feature redundancy and preserve the 100 most common crucial features. Subsequently, the least absolute shrinkage and selection operator (LASSO) was used to identify features demonstrating a high degree

 

of relevance to the outcome variable. The optimal λ value in the LASSO algorithm was identified using 10-fold cross-validation, thus leading to the screening of features with nonzero coefficients (Figure S1).

Finally, the Rad score was calculated based on the identified radiomics features and their coefficients via the LASSO algorithm. The formula for the Rad score was as follows:

$$Rad\ score = \sum_{i=1}^{n} X_i \beta_i + Z \quad [1]$$

where $X_i$ is the radiomics feature selected by the LASSO regression, $\beta_i$ is the regression coefficient of $X_i$, and Z is an intercept.

### *ITH score calculations*

We performed a comprehensive assessment of ITH by integrating local and global radiomics features. Initially, we calculated the consistent radiomics features of every pixel within the nodule area to capture intricate localized details (31). Subsequently, the pixels were clustered according to their inherent local characteristics. These grouped pixels were assigned specific colors corresponding to their cluster labels, thus generating a visually informative map that portrayed the overall pixel distribution pattern. This map enabled easy visualization and aided in quantifying ITH. Pixels that shared identical cluster labels demonstrated similarities in intensity and neighboring textures. Conversely, the distribution of cluster patterns on the label map revealed the extent of heterogeneity within the lesion.

Subsequently, the pGGN regions were divided into distinct subregions based on pixel clustering, which is particularly relevant in the context of tumor heterogeneity. Local entropy calculations were performed on each CT image slice using a 9×9 moving window, and the subregions were clustered with the Calinski-Harabasz method. To precisely determine the requisite number of subgroups within the case sample, we excluded Calinski-Harabasz values that deviated beyond the standard deviation range. Hence, we introduced the ITH score (31-33) as an assessment metric to measure the level of diversity within label maps:

$$ITH\ score = 1 - \frac{1}{S_{total}} \sum_{i=1}^{V} \frac{S_{i,max}}{n_i} \quad [2]$$

where V is the number of clusters, $S_{total}$ is the overall tumor area, and $n_i$ is the number of connected regions, while $S_{i,max}$ represents the maximum area of each connected region within cluster *i*. The two measurable parameters, $n_i$ and $S_{i,max}$, are critical to evaluating the diversity of cluster patterns within each cluster *i*. A more heterogeneous pattern was indicated by an increased number of interconnected regions within each cluster and a reduced maximum area. The ITH score ranged from zero to one, with higher values indicating a label map with increased dispersion (31-33), thus reflecting a broader spectrum of cell compositions and spatial distributions.

### *Statistical analysis*

Statistical analyses were performed using R software version 4.3.2 (The R Foundation of Statistical Computing). Patients diagnosed with lung adenocarcinoma after surgical resection were categorized as having either IAC or AIS/MIA based on histopathology results. Continuous data were analyzed with the independent samples *t*-test or the Mann-Whitney test, while categorical variables were assessed using the chi-square test. Statistical significance was determined at a threshold of P<0.05 (two-tailed).

Three diagnostic models were used to preoperatively predict IAC with pulmonary adenocarcinomas presenting as pGGNs (*Figure 2*). One model comprised imaging findings, one comprised radiomics features, and one comprised the ITH score. Univariate logistic regression identified conventional imaging findings associated with IAC (P<0.1); subsequently, a forward multivariate logistic regression analysis was conducted to identify significant independent variables based on the univariate analysis. The findings are reported as odds ratios (ORs) with corresponding 95% confidence intervals (CIs) and P values. Predicted probability models were formulated using logistic regression coefficients. The Rad and ITH scores were also used to preoperatively predict IAC. The evaluation of each model's performance was conducted through receiver operating characteristic (ROC) curve analysis, with metrics including the area under the curve (AUC), accuracy, sensitivity, specificity, positive predictive value, and negative predictive value being employed. The ROC curves were compared using the DeLong test for statistical significance.

## Results

### *Patient and clinicopathological characteristics*

The study included a total of 575 patients (mean age

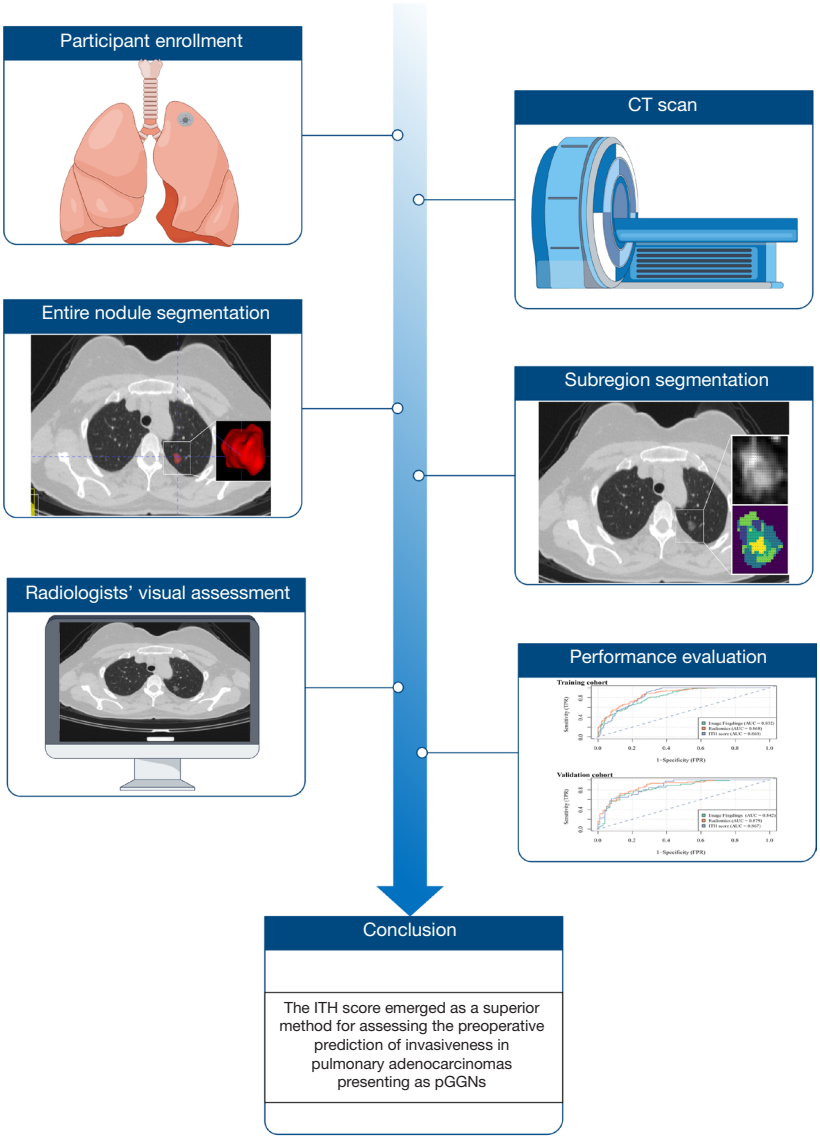


**Figure 2** Comparative study design of three prediction models: conventional imaging findings, radiomics features, and the ITH score. ITH, intratumor heterogeneity; CT, computed tomography; pGGNs, pure ground-glass nodules.

54.79±12.23 years; range, 25–81 years; 29% male) with persistent pGGNs. Of these, 402 and 173 patients were allocated to the training and validation cohorts, respectively. Among the patients, 157 (39.1%) and 71 patients (41%) were pathologically diagnosed with IAC in the training and validation cohorts, respectively. No significant differences were observed in the demographic and clinicoradiological characteristics between the training and validation cohorts (all P values >0.05). The detailed information is provided in *Table 1*.

### *Conventional imaging findings*

*Table 2* presents the results of the univariate and multivariate logistic analyses of the ability of conventional imaging findings to preoperatively predict IAC among pulmonary adenocarcinomas appearing as pGGNs. In the univariate logistic regression analysis, factors including shape, vascular convergence sign, vacuole sign, pleural indentation, age, and CT value were significantly associated with IAC (all P values <0.05). However, in the subsequent multivariate

 

**Table 1** Baseline characteristics of the training and validation cohort

| Variable | Total (n=575) | Training cohort (n=402) | Validation cohort (n=173) | P value |
|---|---|---|---|---|
| Size (mm), mean ± SD | 14.75±5.68 | 14.52±5.57 | 15.26±5.91 | 0.261 |
| Location, n (%) | | | | 0.704 |
| RUL | 200 (34.8) | 136 (33.8) | 64 (37.0) | |
| RLL | 90 (15.7) | 65 (16.2) | 25 (14.5) | |
| RML | 44 (7.7) | 31 (7.7) | 13 (7.5) | |
| LUL | 166 (28.9) | 113 (28.1) | 53 (30.6) | |
| LLL | 75 (13.0) | 57 (14.2) | 18 (10.4) | |
| Boundary, n (%) | | | | 0.515 |
| Ill-defined | 97 (16.9) | 71 (17.7) | 26 (15.0) | |
| Well-defined | 478 (83.1) | 331 (82.3) | 147 (85.0) | |
| Shape, n (%) | | | | 0.818 |
| Irregular | 165 (28.7) | 117 (29.1) | 48 (27.7) | |
| Regular | 410 (71.3) | 285 (70.9) | 125 (72.3) | |
| Lobulation, n (%) | | | | 0.913 |
| Absence | 372 (64.7) | 259 (64.4) | 113 (65.3) | |
| Presence | 203 (35.3) | 143 (35.6) | 60 (34.7) | |
| Spiculation, n (%) | | | | 1.000 |
| Absence | 422 (73.4) | 295 (73.4) | 127 (73.4) | |
| Presence | 153 (26.6) | 107 (26.6) | 46 (26.6) | |
| Vascular convergence sign, n (%) | | | | 1.000 |
| Absence | 140 (24.3) | 98 (24.4) | 42 (24.3) | |
| Presence | 435 (75.7) | 304 (75.6) | 131 (75.7) | |
| Vacuole sign, n (%) | | | | 0.82 |
| Absence | 494 (85.9) | 344 (85.6) | 150 (86.7) | |
| Presence | 81 (14.1) | 58 (14.4) | 23 (13.3) | |
| Pleural indentation, n (%) | | | | 0.682 |
| Absence | 350 (60.9) | 242 (60.2) | 108 (62.4) | |
| Presence | 225 (39.1) | 160 (39.8) | 65 (37.6) | |
| Sex, n (%) | | | | 0.727 |
| Male | 167 (29.0) | 119 (29.6) | 48 (27.7) | |
| Female | 408 (71.0) | 283 (70.4) | 125 (72.3) | |
| Age (years), mean ± SD | 54.79±12.23 | 54.52±12.53 | 55.45±11.53 | 0.53 |
| CT value (HU), mean ± SD | −596.93±98.38 | −595.26±96.68 | −600.79±102.42 | 0.48 |
| Pathologic diagnosis, n (%) | | | | 0.724 |
| AIS/MIA | 347 (60.3) | 245 (60.9) | 102 (59.0) | |
| IAC | 228 (39.7) | 157 (39.1) | 71 (41.0) | |

LUL, left upper lobe; LLL, left lower lobe; RUL, right upper lobe; RML, right middle lobe; RLL, right lower lobe; IAC, invasive lung adenocarcinoma; AIS, adenocarcinoma in situ; MIA, minimally invasive adenocarcinoma; CT, computed tomography; HU, Hounsfield unit.

**Table 2** Univariate and multivariate logistic analysis for distinguishing IAC from AIC/MIA in pulmonary adenocarcinomas presenting as pGGNs

| Variable | AIC/MIA | IAC | Univariate | | Multivariate | |
|---|---|---|---|---|---|---|
| | | | OR (95% CI) | P | OR (95% CI) | P |
| Size (mm), mean ± SD | 12.0±4.4 | 18.5±4.9 | 1.31 (1.24–1.38) | <0.001 | 1.28 (1.20–1.36) | <0.001 |
| Location, n (%) | | | | | | |
| RUL | 82 (33.5) | 54 (34.4) | | | | |
| RLL | 42 (17.1) | 23 (14.6) | 0.83 (0.45–1.54) | 0.556 | | |
| RML | 21 (8.6) | 10 (6.4) | 0.72 (0.32–1.65) | 0.443 | | |
| LUL | 62 (25.3) | 51 (32.5) | 1.25 (0.75–2.07) | 0.388 | | |
| LLL | 38 (15.5) | 19 (12.1) | 0.76 (0.40–1.45) | 0.406 | | |
| Boundary, n (%) | | | | | | |
| Ill-defined | 40 (16.3) | 31 (19.7) | | | | |
| Well-defined | 205 (83.7) | 126 (80.3) | 0.79 (0.47–1.33) | 0.381 | | |
| Shape, n (%) | | | | | | |
| Irregular | 53 (21.6) | 64 (40.8) | | | | |
| Regular | 192 (78.4) | 93 (59.2) | 0.40 (0.26–0.62) | <0.001 | 1.24 (0.69–2.25) | 0.468 |
| Lobulation, n (%) | | | | | | |
| Absence | 160 (65.3) | 99 (63.1) | | | | |
| Presence | 85 (34.7) | 58 (36.9) | 1.10 (0.73–1.67) | 0.646 | | |
| Spiculation, n (%) | | | | | | |
| Absence | 188 (76.7) | 107 (68.2) | | | | |
| Presence | 57 (23.3) | 50 (31.8) | 1.54 (0.98–2.41) | 0.058 | | |
| Vascular convergence sign, n (%) | | | | | | |
| Absence | 68 (27.8) | 30 (19.1) | | | | |
| Presence | 177 (72.2) | 127 (80.9) | 1.63 (1.00–2.64) | 0.049 | 1.00 (0.54–1.87) | 0.991 |
| Vacuole sign, n (%) | | | | | | |
| Absence | 224 (91.4) | 120 (76.4) | | | | |
| Presence | 21 (8.6) | 37 (23.6) | 3.29 (1.84–5.87) | <0.001 | 1.87 (0.90–3.90) | 0.092 |
| Pleural indentation, n (%) | | | | | | |
| Absence | 168 (68.6) | 74 (47.1) | | | | |
| Presence | 77 (31.4) | 83 (52.9) | 2.45 (1.62–3.70) | <0.001 | 1.32 (0.78–2.24) | 0.297 |
| Sex, n (%) | | | | | | |
| Male | 66 (26.9) | 53 (33.8) | | | | |
| Female | 179 (73.1) | 104 (66.2) | 0.72 (0.47–1.12) | 0.145 | | |
| Age (years), mean ± SD | 52.2±13.5 | 58.2±9.9 | 1.04 (1.02–1.06) | <0.001 | 1.01 (0.98–1.03) | 0.633 |
| CT value (HU), mean ± SD | –617.5±88.0 | –560.6±99.6 | 1.01 (1.00–1.01) | <0.001 | 1.01 (1.00–1.01) | <0.001 |

LUL, left upper lobe; LLL, left lower lobe; RUL, right upper lobe; RML, right middle lobe; RLL, right lower lobe; IAC, invasive lung adenocarcinoma; AIS, adenocarcinoma in situ; MIA, minimally invasive adenocarcinoma; pGGN, pure ground-glass nodule; SD, standard deviation; OR, odds ratio; CI, confidence interval; CT, computed tomography; HU, Hounsfield unit.

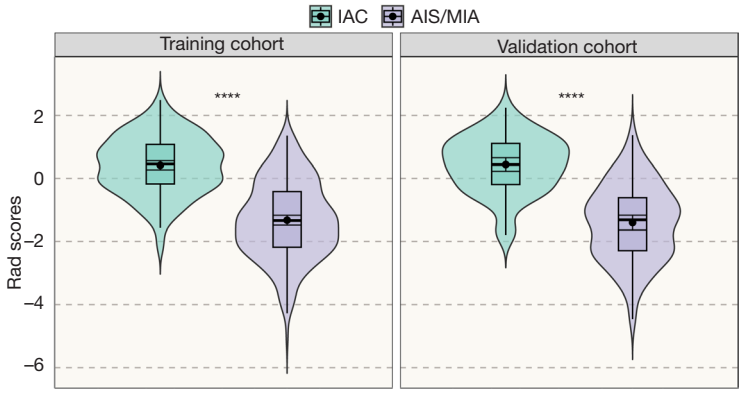


**Figure 3** Comparison of the radiomics scores (Rad scores) of the IAC and AIS/MIA groups. ****, P<0.001. IAC, invasive adenocarcinoma; AIS, adenocarcinoma in situ; MIA, minimally invasive adenocarcinoma.

logistic regression analysis, only tumor size (OR 1.28; 95% CI: 1.20–1.36; P<0.001) and CT value (OR 1.01; 95% CI: 1.00–1.01; P<0.001) emerged as independent predictors capable of differentiating IAC from AIS/MIA.

### *Radiomics model*

LASSO regression identified 10 radiomics features that could preoperatively predict IAC with pulmonary adenocarcinomas presenting as pGGNs (Figure S2). The Rad score of the IAC group, calculated based on these selected radiomics features and their coefficients via LASSO regression, was higher than that of the AIS/MIA group in both the training and validation cohorts (all P values <0.05) (*Figure 3*). To further assess the robustness of the radiomics model, five-fold cross-validation was performed. The AUCs for folds one, two, three, four, and five were 0.879, 0.861, 0.845, 0.849, and 0.814, respectively (mean AUC 0.850). The AUC values remained relatively stable across the folds (Figure S3).

### *Application of ITH score*

In this study, we developed and assessed a methodology for calculating the voxel composition of small patches within pGGNs and subsequently clustered these patches to identify subregions exhibiting analogous patterns. This methodology facilitates a comprehensive analysis of the textural and biological attributes within these specific regions, thereby enabling the quantification of pGGN heterogeneity at a higher resolution. Consequently, this approach provides deeper insights into the potential pathological implications of clustered patches. The data obtained from these clusters, along with their associated texture information, were subsequently used to quantify ITH (*Figure 4*).

We found that the ITH score generated to quantify pGGN heterogeneity in the CT images of the IAC group was higher than that of the AIS/MIA group in both the training and validation cohorts (all P values <0.05) (*Figure 5*).

### *Evaluation of model performance*

The ROC curves for imaging findings, radiomics features, and ITH scores of the IAC and AIS/MIA groups in both the training and validation cohorts are illustrated in *Figure 6*. In distinguishing between IAC and AIS/MIA in pulmonary adenocarcinomas presenting as pGGNs, conventional imaging yielding AUC values of 0.832 (95% CI: 0.794–0.871) and 0.842 (95% CI: 0.783–0.901) for the training and validation cohorts, respectively. These values were inferior to those of the radiomics features, which yielded AUC values of 0.868 (95% CI: 0.835–0.902) for the training cohort (DeLong P=0.008) and 0.879 (95% CI: 0.829–0.929) for the validation cohort (DeLong test P=0.007). Additionally, the AUC values of conventional imaging findings were inferior to those of the ITH score, which yielded AUC values of 0.860 (95% CI: 0.825–0.895) for the training cohort (DeLong test P=0.019) and 0.867 (95% CI: 0.815–0.918) for the validation cohort (DeLong test P=0.045). The diagnostic efficacy of the ITH score was comparable with that of radiomics features, with no significant difference between the ROC curves of the training (DeLong test P=0.635) and validation cohorts (DeLong test P=0.686) (*Table 3*).

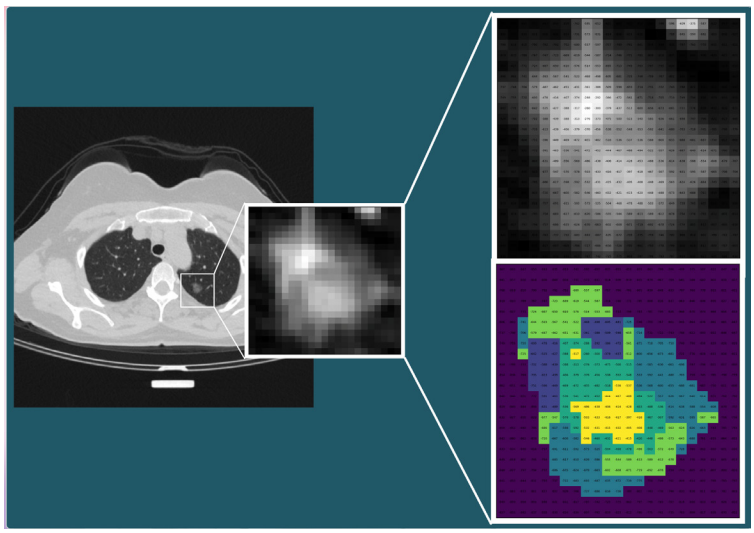

**Figure 4** Subregions were identified by clustering image patches to quantify intratumor heterogeneity.

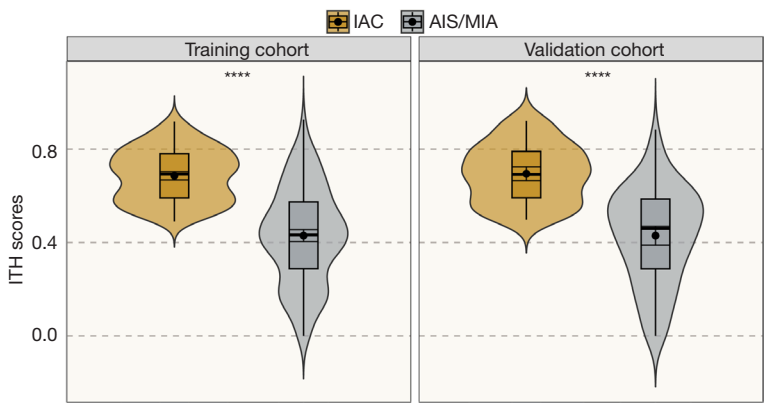


**Figure 5** Comparison of ITH scores of the IAC and AIS/MIA groups. ****, P<0.001. IAC, invasive adenocarcinoma; AIS, adenocarcinoma in situ; MIA, minimally invasive adenocarcinoma; ITH, intratumor heterogeneity.

## Discussion

Tumor heterogeneity plays a pivotal role in shaping the malignancy and biological characteristics of tumors, underscoring the significance of quantifying preoperative evaluation of ITH in the assessment of pGGN invasiveness. This study examined the initial application of preoperative CT imaging for quantifying ITH in persistent pGGNs to assess pathological invasiveness. The ITH score, which is an amalgamation of local textural features and overall pixel distribution patterns, exhibited outstanding diagnostic accuracy. The ITH score demonstrated superior performance compared to conventional imaging findings and was comparable to radiomics features.

In this study, univariate analysis indicated that various conventional imaging findings, including shape, vascular convergence sign, vacuole sign, pleural indentation, age, and mean CT value, were associated with IAC (all P values <0.05). However, multivariate logistic analysis indicated that only tumor size (OR 1.28, 95% CI: 1.20–1.36; P<0.001) and CT value (OR 1.01; 95% CI: 1.00–1.01; P<0.001) were independent predictors that could distinguish IAC from AIS/MIA. A meta-analysis conducted by Yang *et al.* (23) demonstrated a noteworthy disparity in the mean CT values of pGGNs with IAC and AIS/MIA. Similar results were obtained in a meta-analysis by He *et al.* (34). In contrast,

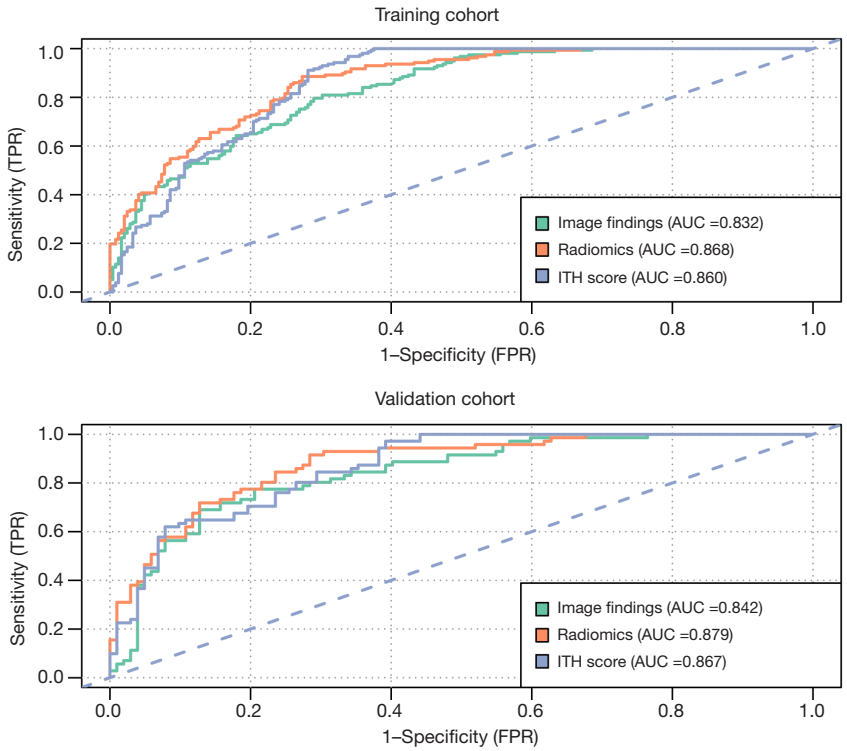


**Figure 6** ROC curves depicting the ability of imaging findings, radiomics features, and the ITH score in predicting invasiveness. ROC, receiver operating characteristic; ITH, intratumor heterogeneity; AUC, area under the curve; TPR, true positive rate; FPR, false positive rate.

**Table 3** Diagnostic performance of models in distinguishing IAC from AIS/MIA

| Model | Area under the curve (95% CI) | Accuracy (95% CI) | Sensitivity (95% CI) | Specificity (95% CI) | Positive predictive value (95% CI) | Negative predictive value (95% CI) |
|---|---|---|---|---|---|---|
| Training cohort | | | | | | |
| Imaging findings | 0.832 (0.794–0.871) | 0.741 (0.740–0.742) | 0.809 (0.747–0.870) | 0.698 (0.640–0.755) | 0.632 (0.565–0.699) | 0.851 (0.801–0.900) |
| Radiomics | 0.868 (0.835–0.902) | 0.789 (0.788–0.789) | 0.885 (0.836–0.935) | 0.727 (0.671–0.782) | 0.675 (0.611–0.739) | 0.908 (0.868–0.949) |
| ITH score | 0.860 (0.825–0.895) | 0.781 (0.780–0.782) | 0.968 (0.941–0.996) | 0.661 (0.602–0.720) | 0.647 (0.586–0.708) | 0.970 (0.944–0.996) |
| Validation cohort | | | | | | |
| Imaging findings | 0.842 (0.783–0.901) | 0.786 (0.784–0.788) | 0.775 (0.677–0.872) | 0.794 (0.716–0.873) | 0.724 (0.623–0.824) | 0.835 (0.761–0.909) |
| Radiomics | 0.879 (0.829–0.929) | 0.798 (0.796–0.800) | 0.915 (0.851–0.980) | 0.716 (0.628–0.803) | 0.691 (0.598–0.785) | 0.924 (0.866–0.982) |
| ITH score | 0.867 (0.815–0.918) | 0.757 (0.755–0.759) | 0.972 (0.933–1.000) | 0.608 (0.513–0.703) | 0.633 (0.543–0.724) | 0.969 (0.926–1.011) |

IAC, invasive lung adenocarcinoma; AIS, adenocarcinoma in situ; MIA, minimally invasive adenocarcinoma; ITH, intratumor heterogeneity; CI, confidence interval.

Fu *et al.* (18) conducted a study involving 432 patients with pGGNs and concluded that mean CT value is not a reliable independent predictor for pathological invasion of pGGNs. This inconsistency may be explained by the effect of myofibroblast matrix thickening induced by tumor cell infiltration on the mean CT value because increased invasiveness is correlated with an increased mean CT value. Conversely, a reduction in air content within the cavity due to alveolar collapse may result in an elevated mean CT value (35). Hence, the ability of mean CT value to detect pGGN invasiveness remains unclear, as highlighted by the findings our study, in which the mean CT value could distinguish the invasiveness of pGGNs but produced a low OR. In contrast to mean CT value, tumor size is widely acknowledged as a criterion for evaluating the invasiveness of pGGNs (17-19) and is thus included in the guidelines outlined in the eighth edition of the TNM staging protocols (15).

The ITH score provides an objective evaluation of heterogeneity by incorporating both pixel characteristics and their spatial distributions. This method represents a significant advancement in capturing multiscale tumor heterogeneity by integrating local and global radiomics information (30-33). In our study, the performance of ITH score was superior to that of conventional imaging findings and comparable with that of radiomics features in both the training and validation cohorts. The ITH score offers unique advantages over radiomics features because it provides more abundant and objective information and reduces the subjective interpretation inherent in conventional imaging findings. Additionally, initial radiomics features such as first-order statistics, wavelet attributes, and textures can be susceptible to variations in image capture methods (36). Conversely, the ITH score consolidates features by clustering labeling maps, thus ensuring consistency across diverse tumor images while preserving intratumor diversity. This approach enables a reliable comparison of ITH scores across various medical institutions. Although radiomics models usually rely on regression techniques such as LASSO for specific tasks, the ITH score is derived using unsupervised machine learning, thereby eliminating the need for training (32,33). The intuitive cluster patterns observed in the labeling maps enhanced the interpretability of the ITH score.

Some limitations to this study should be noted. First, although our findings suggest a connection between the ITH score and the invasiveness of pulmonary adenocarcinomas presenting as pGGNs, further exploration of the broader clinical implications of the ITH score, particularly its relevance to follow-up decision-making, determination of the extent of surgical resection, and prognosis, is required. Second, our study did not further examine gene immunomics and genomics to evaluate the efficacy of the ITH score, which limits our understanding of the relationship between ITH scores and histological traits. Third, although we implemented a comprehensive image preprocessing pipeline to address the issue of variability in CT scanner devices and parameters, the influence of these factors on radiomic features and the ITH score could not be excluded. Finally, due to the retrospective nature of the study, bias in participant selection might have occurred, which could limit the generalizability of the results.

## Conclusions

In this preliminary study, we introduced the novel concept of a comprehensive ITH score that can be used to assess the heterogeneity of persistent pGGNs. The ITH score demonstrated superior performance compared to conventional imaging findings and may be an alternative to the radiomics protocol due to its unique advantages. Furthermore, the ITH score could be used to inform surgical strategies and posttreatment monitoring protocols for lung adenocarcinomas that manifest as persistent pGGNs.

## Acknowledgments

*Funding:* This study was supported by the President Foundation of Nanfang Hospital, Southern Medical University (Nos. 2022B016 and 2022B030 to H.Q., Y.C., H.L., D.H., and H.C.), and the Postgraduate Scientific Research Innovation Project of Xiangtan University (No. CX20240599 to Z.Z.).

## Footnote

*Reporting Checklist:* The authors have completed the TRIPOD reporting checklist. Available at https://qims.amegroups.com/article/view/10.21037/qims-24-734/rc

*Conflicts of Interest:* All authors have completed the ICMJE uniform disclosure form (available at https://qims.amegroups.com/article/view/10.21037/qims-24-734/coif). H.Q., Y.C., H.L., D.H., and H.C. report that this study was supported by the President Foundation of Nanfang Hospital, Southern Medical University (Nos. 2022B016 and

 

2022B030). Z.Z. reports that this study was supported by the Postgraduate Scientific Research Innovation Project of Xiangtan University (No. CX20240599). The other authors have no other conflicts of interest to declare.

*Ethical Statement:* The authors are accountable for all aspects of the work in ensuring that questions related to the accuracy or integrity of any part of the work are appropriately investigated and resolved. This study was conducted in compliance with the Helsinki Declaration (as revised in 2013). Ethical approval for this multicenter, cancer registry-based study was obtained from the institutional ethics committees of the Xiangtan Central Hospital (No. 2021-07-009), Affiliated Hospital of Guilin Medical University (No. 2023YJSLL-121), and the Affiliated Hospital of Southwest Medical University (No. KY2020147). Given the retrospective design of the study, the necessity for obtaining written informed consent from participants was waived.



## References

1. Sung H, Ferlay J, Siegel RL, Laversanne M, Soerjomataram I, Jemal A, Bray F. Global Cancer Statistics 2020: GLOBOCAN Estimates of Incidence and Mortality Worldwide for 36 Cancers in 185 Countries. CA Cancer J Clin 2021;71:209-49.
2. Aberle DR, Adams AM, Berg CD, Black WC, Clapp JD, Fagerstrom RM, Gareen IF, Gatsonis C, Marcus PM, Sicks JD. Reduced lung-cancer mortality with low-dose computed tomographic screening. N Engl J Med 2011;365:395-409.
3. Zhang Y, Jheon S, Li H, Zhang H, Xie Y, Qian B, Lin K, Wang S, Fu C, Hu H, Zheng Y, Li Y, Chen H. Results of low-dose computed tomography as a regular health examination among Chinese hospital employees. J Thorac Cardiovasc Surg 2020;160:824-831.e4.
4. Kobayashi Y, Mitsudomi T, Sakao Y, Yatabe Y. Genetic features of pulmonary adenocarcinoma presenting with ground-glass nodules: the differences between nodules with and without growth. Ann Oncol 2015;26:156-61.
5. Lin MW, Su KY, Su TJ, Chang CC, Lin JW, Lee YH, Yu SL, Chen JS, Hsieh MS. Clinicopathological and genomic comparisons between different histologic components in combined small cell lung cancer and non-small cell lung cancer. Lung Cancer 2018;125:282-90.
6. Lee GD, Park CH, Park HS, Byun MK, Lee IJ, Kim TH, Lee S. Lung Adenocarcinoma Invasiveness Risk in Pure Ground-Glass Opacity Lung Nodules Smaller than 2 cm. Thorac Cardiovasc Surg 2019;67:321-8.
7. Suzuki K, Koike T, Asakawa T, Kusumoto M, Asamura H, Nagai K, Tada H, Mitsudomi T, Tsuboi M, Shibata T, Fukuda H, Kato H; Japan Lung Cancer Surgical Study Group (JCOG LCSSG). A prospective radiological study of thin-section computed tomography to predict pathological noninvasiveness in peripheral clinical IA lung cancer (Japan Clinical Oncology Group 0201). J Thorac Oncol 2011;6:751-6.
8. Liu J, Yang X, Li Y, Xu H, He C, Qing H, Ren J, Zhou P. Development and validation of qualitative and quantitative models to predict invasiveness of lung adenocarcinomas manifesting as pure ground-glass nodules based on low-dose computed tomography during lung cancer screening. Quant Imaging Med Surg 2022;12:2917-31.
9. Zhang H, Wang D, Li W, Tian Z, Ma L, Guo J, Wang Y, Sun X, Ma X, Ma L, Zhu L. Artificial intelligence system-based histogram analysis of computed tomography features to predict tumor invasiveness of ground-glass nodules. Quant Imaging Med Surg 2023;13:5783-95.
10. Cohen JG, Ferretti GR. Pure ground-glass nodules: are they really indolent? J Thorac Dis 2017;9:2839-42.
11. Qi L, Xue K, Li C, He W, Mao D, Xiao L, Hua Y, Li M. Analysis of CT morphologic features and attenuation for differentiating among transient lesions, atypical adenomatous hyperplasia, adenocarcinoma in situ, minimally invasive and invasive adenocarcinoma presenting as pure ground-glass nodules. Sci Rep 2019;9:14586.
12. Jin X, Zhao SH, Gao J, Wang DJ, Wu J, Wu CC, Chang RP, Ju HY. CT characteristics and pathological implications of early stage (T1N0M0) lung adenocarcinoma with pure ground-glass opacity. Eur Radiol 2015;25:2532-40.
13. Yotsukura M, Asamura H, Motoi N, Kashima J, Yoshida Y, Nakagawa K, Shiraishi K, Kohno T, Yatabe Y, Watanabe SI. Long-Term Prognosis of Patients With Resected Adenocarcinoma In Situ and Minimally Invasive Adenocarcinoma of the Lung. J Thorac Oncol

2021;16:1312-20.
14. Watanabe Y, Hattori A, Nojiri S, Matsunaga T, Takamochi K, Oh S, Suzuki K. Clinical impact of a small component of ground-glass opacity in solid-dominant clinical stage IA non-small cell lung cancer. J Thorac Cardiovasc Surg 2022;163:791-801.e4.
15. Van Schil PE, Asamura H, Rusch VW, Mitsudomi T, Tsuboi M, Brambilla E, Travis WD. Surgical implications of the new IASLC/ATS/ERS adenocarcinoma classification. Eur Respir J 2012;39:478-86.
16. Ito H, Nakayama H, Murakami S, Yokose T, Katayama K, Miyata Y, Okada M. Does the histologic predominance of pathological stage IA lung adenocarcinoma influence the extent of resection? Gen Thorac Cardiovasc Surg 2017;65:512-8.
17. Liu J, Yang X, Li Y, Xu H, He C, Zhou P, Qing H. Predicting the Invasiveness of Pulmonary Adenocarcinomas in Pure Ground-Glass Nodules Using the Nodule Diameter: A Systematic Review, Meta-Analysis, and Validation in an Independent Cohort. Diagnostics (Basel) 2024.
18. Fu F, Zhang Y, Wang S, Li Y, Wang Z, Hu H, Chen H. Computed tomography density is not associated with pathological tumor invasion for pure ground-glass nodules. J Thorac Cardiovasc Surg 2021;162:451-459.e3.
19. Zuo Z, Wang P, Zeng W, Qi W, Zhang W. Measuring pure ground-glass nodules on computed tomography: assessing agreement between a commercially available deep learning algorithm and radiologists' readings. Acta Radiol 2023;64:1422-30.
20. Ichinose J, Kawaguchi Y, Nakao M, Matsuura Y, Okumura S, Ninomiya H, Oikado K, Nishio M, Mun M. Utility of Maximum CT Value in Predicting the Invasiveness of Pure Ground-Glass Nodules. Clin Lung Cancer 2020;21:281-7.
21. Zhou QJ, Zheng ZC, Zhu YQ, Lu PJ, Huang J, Ye JD, Zhang J, Lu S, Luo QQ. Tumor invasiveness defined by IASLC/ATS/ERS classification of ground-glass nodules can be predicted by quantitative CT parameters. J Thorac Dis 2017;9:1190-200.
22. Chu ZG, Li WJ, Fu BJ, Lv FJ. CT Characteristics for Predicting Invasiveness in Pulmonary Pure Ground-Glass Nodules. AJR Am J Roentgenol 2020;215:351-8.
23. Yang Y, Xu J, Wang W, Zhao J, Yang Y, Wang B, Ye L. Meta-analysis of the correlation between CT-based features and invasive properties of pure ground-glass nodules. Asian J Surg 2023;46:3405-16.
24. Park J, Doo KW, Sung YE, Jung JI, Chang S. Computed Tomography Findings for Predicting Invasiveness of Lung Adenocarcinomas Manifesting as Pure Ground-Glass Nodules. Can Assoc Radiol J 2023;74:137-46.
25. Chen M, Copley SJ, Viola P, Lu H, Aboagye EO. Radiomics and artificial intelligence for precision medicine in lung cancer treatment. Semin Cancer Biol 2023;93:97-113.
26. Fan L, Fang M, Li Z, Tu W, Wang S, Chen W, Tian J, Dong D, Liu S. Radiomics signature: a biomarker for the preoperative discrimination of lung invasive adenocarcinoma manifesting as a ground-glass nodule. Eur Radiol 2019;29:889-97.
27. Kao TN, Hsieh MS, Chen LW, Yang CJ, Chuang CC, Chiang XH, Chen YC, Lee YH, Hsu HH, Chen CM, Lin MW, Chen JS. CT-Based Radiomic Analysis for Preoperative Prediction of Tumor Invasiveness in Lung Adenocarcinoma Presenting as Pure Ground-Glass Nodule. Cancers (Basel) 2022.
28. Wu L, Gao C, Ye J, Tao J, Wang N, Pang P, Xiang P, Xu M. The value of various peritumoral radiomic features in differentiating the invasiveness of adenocarcinoma manifesting as ground-glass nodules. Eur Radiol 2021;31:9030-7.
29. Napel S, Mu W, Jardim-Perassi BV, Aerts HJWL, Gillies RJ. Quantitative imaging of cancer in the postgenomic era: Radio(geno)mics, deep learning, and habitats. Cancer 2018;124:4633-49.
30. Depeursinge A. Chapter 2 - Multiscale and Multidirectional Biomedical Texture Analysis: Finding the Needle in the Haystack. In: Biomedical Texture Analysis: Fundamentals, Applications and Tools. Academic Press; 2017:29-53.
31. van Griethuysen JJM, Fedorov A, Parmar C, Hosny A, Aucoin N, Narayan V, Beets-Tan RGH, Fillion-Robin JC, Pieper S, Aerts HJWL. Computational Radiomics System to Decode the Radiographic Phenotype. Cancer Res 2017;77:e104-7.
32. Li J, Qiu Z, Zhang C, Chen S, Wang M, Meng Q, Lu H, Wei L, Lv H, Zhong W, Zhang X. ITHscore: comprehensive quantification of intra-tumor heterogeneity in NSCLC by multi-scale radiomic features. Eur Radiol 2023;33:893-903.
33. Zhang J, Sha J, Liu W, Zhou Y, Liu H, Zuo Z. Quantification of Intratumoral Heterogeneity: Distinguishing Histological Subtypes in Clinical T1 Stage Lung Adenocarcinoma Presenting as Pure Ground-Glass Nodules on Computed Tomography. Acad Radiol 2024;31:4244-55.
34. He S, Chen C, Wang Z, Yu X, Liu S, Huang Z, Chen

 

C, Liang Z, Chen C. The use of the mean computed-tomography value to predict the invasiveness of ground-glass nodules: A meta-analysis. Asian J Surg 2023;46:677-82.
35. She Y, Zhao L, Dai C, Ren Y, Zha J, Xie H, Jiang S, Shi J, Shi S, Shi W, Yu B, Jiang G, Fei K, Chen Y, Chen C. Preoperative nomogram for identifying invasive pulmonary adenocarcinoma in patients with pure ground-glass nodule: A multi-institutional study. Oncotarget 2017;8:17229-38.
36. Traverso A, Wee L, Dekker A, Gillies R. Repeatability and Reproducibility of Radiomic Features: A Systematic Review. Int J Radiat Oncol Biol Phys 2018;102:1143-58.

**Cite this article as:** Qi H, Zuo Z, Lin S, Chen Y, Li H, Hu D, Zhou Y, Qi W, Chen H. Assessment of intratumor heterogeneity for preoperatively predicting the invasiveness of pulmonary adenocarcinomas manifesting as pure ground-glass nodules. Quant Imaging Med Surg 2025;15(1):272-286. doi: 10.21037/qims-24-734